Contents lists available at **ACERP**

Advanced Ceramics Progress

Materials and Energy Research Center

MERC

Journal Homepage: www.acerp.ir

Original Research Article

Oxidation Behavior of Spark Plasma Sintered HfB₂-SiC-Graphite Composite at 1400 °C

Mohammad Sakvand [a], Maryam Shojaie-Bahaabad [b, ∗], Leila Nikzad [c]

[a] MSc Student , Faculty of Chemical and Materials Engineering, Shahrood University of Technology, Shahrood, Semnan, Iran
[b] Assistant Professor, Faculty of Chemical and Materials Engineering, Shahrood University of Technology, Shahrood, Semnan, Iran
[c] Assistant Professor, Department of Ceramics, Materials, and Energy Research Center (MERC), Meshkindasht, Alborz, Iran

∗ Corresponding Author Email: mshojaieb@shahroodut.ac.ir (M. Shojaie-Bahaabad)   URL: https://www.acerp.ir/article_147536.html

A R T I C L E   I N F O

A B S T R A C T

The current study aims to fabricate the HfB₂-SiC-graphite composite through Spark Plasma Sintering (SPS) method at 1950 °C for 10 min. The oxidation behavior of the prepared composites was investigated at 1400 °C and different times of 4, 8, 12, and 16 h. In addition, the weight changes and thickness of the generated oxide layer were measured. The relative density, hardness, toughness, and strength of the composite made through the SPS method were calculated as 99.39 %, 10.16 GPa, 4.73 MPa.m$^{1/2}$, and 464.12 MPa, respectively. The oxidation kinetic results of the composite exhibited linear-parabolic behavior. The chemical reaction during the oxidation process controlled the oxidation rate after 8 h. Followed by oxidation for more 12 h, the thickness of the oxide scale slowly increased, thus following a parabolic trend as a result of a decrease in the oxygen diffusion when HfO_xC_y and SiO_xC_y phases were formed. Therefore, it was concluded that the oxygen diffusion rate could control the oxidation process.

1. INTRODUCTION

Ultra-High Temperature Ceramics (UHTCs) consist of nitrides, carbides, and borides of transition metal [1-3]. UHTCs have recently drawn researchers' attention owing to their ablation resistance and high oxidation at quite high temperatures while applied in Thermal Protection Systems (TPSs) such as nosecone, propulsion system, sharp leading edge, and rocket nozzle [3]. Among all types of UHTCs, HfB₂ has received considerbale attention compared to other deborides due to its advantagous characteristics such as higher melting temperature (3380 °C), thermal conductivity (104 W/m.K), Young's modulus (480 GPa), high resistance against oxidation, good hardness (28 GPa), and high chemical resistance [4].

Owing to the robust covalent bonds, low self-diffusion coefficient, presence of oxygen contaminants of non-oxide raw materials, and high temperature, mechanical pressure is often require d during a long period to achieve full density [3].

Numerous approaches such as hot pressing, pressureless sintering, reactive hot pressing, and plasma spark sintering, to name a few, are commonly used used

for sintering HfB_2 composites [5-7].

The spark plasma process requires low sintering temperature and shorter soaking time due to its higher heating rate than that of other methods [3]. Therefore, it is possible to make ceramics at high temperatures and speeds, i.e., a homogeneous fine grain structure with full density that requires less sintering. Upon adding the metallic additives (Fe, Ni, Co, W), carbides (SiC, HfC, WC, VC), nitrides (AlN, HfN, Si_3N_4), and desilicides ($MoSi_2$, $HfSi_2$, $TiSi_2$, $TaSi_2$) [3, 8-10], both sinterability and mechanical characteristics of HfB_2 ceramics will be greatly improved.

Some recent studies pointed out to the necessity of the presence of 10-30 vol. % SiC to achieve high oxidation resistance at high temperatures. Silicon carbide can improve the oxidation resistance of HfB_2 ceramics by forming a B_2O_3-SiO_2 glass layer above 1200 °C on the surface of the HfB_2 matrix and inhibition oxygen diffusion into the bulk [11]. Followed by the oxidation of HfB_2 at 800 °C, HfO_2 (s) and B_2O_3 (l) will be formed. At 1200 °C, SiC is oxidized, and the liquid-formed SiO_2 react with B_2O_3 (l) to produce borosilicate layer on the surface.

This borosilicate layer fascilitates passive oxidation, which results in a parabolic mass gain, and decreases the oxidation rate of HfB_2-SiC composites compared to pure HfB_2 [12,13]. In this regard, many studies have been conducted on the optimization of the properties of HfB_2-SiC ceramic composite compound and coatings in the past years [14-16]. However, low fracture toughness of HfB_2-SiC ceramic composites is an obstacle to their wide applications, especially in harsh environments. It was observed that both sinterability and fracture toughness of HfB_2-SiC composites were enhanced by adding geraphen or short carbon fibers [17,18].

To the best of the authors' knowledge, the impact of SiC and graphite co-addition on the densification as well as the mechanical and oxidation behavior of HfB_2 ceramics produced through the SPS method has not been examined yet. The previous study on the effect of the graphite addition on the mechanical properties of HfB_2-30 vol. % SiC composites confirmed the good mechanical properties of the HfB_2-20 vol. % SiC-6 vol. % graphite composite. In this research, the spark plasma sintering method was employed to fabricate HfB_2-30 vol. % SiC composite combined with 6 vol. % graphite. In addition, both densification and oxidation behavior as well as the mechanical characteristics of the mentioned composite at 1400 °C for 4, 8, 12, and 16 h were studied.

2. MATERIALS AND METHODS

Commercial HfB_2, SiC, and graphite flakes were used to synthesize the HfB_2-20 vol. % SiC-graphite (6 vol. %)

composite. Table 1 shows the properties of the starting powders.

TABLE 1. Characteristics of starting materials

Materials	Supplier	Dimension	Purity
HfB_2	Beijing Cerametek Materials Co., China	$D < 2 \, \mu m$	97 %
SiC	Xuzhou Co., China	$D < 10 \, \mu m$	99 %
Graphite	Qingdao Tiansheng Graphite Co.,China	$D < 50 \, nm$ $L < 30 \, \mu m$	99.9 %

In order to mill HfB_2 and SiC powder mixtures, first, high-energy planetary milling was applied using balls and a WC-Co cup at 300 rpm in ethanol medium with the ball-powder weight ratio of 10:1 for 3 h. The graphite nano-flakes were then ultrasonically stirred in 100 mL diluted ethanol for 1 h, and the mixture of HfB_2 and SiC powder was added to the slurry and stirred for 30 min. Next, the slurry was dried on a hot plate equipped with magnetic stirring at 60 °C for 2 h. HfB_2-30SiC-graphite composites were fabricated through the SPS method (Nanozint 10i, Khala Poushan Felez Co., Iran) at 1950 °C for 10 min under 40 MPa pressure in the vacuum of 0.05 mbar.

The relative density of the composite and porosity values were calculated in the distilled water using Archimedes technique. The theoretical density was also measured based on the mixture law using the theoretical density of 11.2 g/cm^3 for HfB_2, 3.2 g/cm^3 for SiC, and 2.26 g/cm^3 for graphite. Phase analysis of composites was conducted using X-Ray Diffraction (XRD, Philips, Model: X'Pert MPD, Tube: Co, and λ: 1.78897 Å) pattern. Further, the surface and microstructure of the composite were examined using Field Emission Scanning Electron Microscope (FESEM, TESCAN, Model: MIRA) equipped with Energy Dispersive X-Ray spectroscopy (EDS) detector. The microstructure of the composite was investigated neglecting the thermal or chemical etching. The average grain size of the composite was measured by MIP Cloud software. The composite hardness was also measured using a Vickers hardness tester under 1 kg at the loading time of 10 s. In addition, the toughness of the composites was calculated through Equation (1) [14]:

$$K_{IC} = 0.073 \, (P/c^{1.5}) \qquad (1)$$

where K_{IC} denotes the fracture toughness (MPa.m$^{1/2}$), P the applied load (N), and c the average half-length of the crack (μm). The composite flexural strength was evaluated by a three-point flexural machine (Zwick Roell SP600, Germany) at the loading rate of 0.05 mm/min. The oxidation tests were carried out in an electric furnace at 1400 °C for 4, 8, 12, and 16 h. The composite oxidation resistance was evaluated considering the weight changes and thickness of the oxide layer after oxidation.

3. RESULTS AND DISCUSSION

Figure 1 shows the ram displacement and densification behavior of HfB_2-30 SiC-graphite composite during the SPS process.
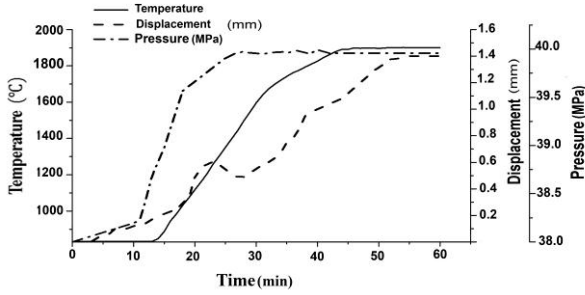

Figure 1. Displacement-Temperature-Time (DTT) curves of the HfB_2-30 SiC-graphite composite

The compaction processes include three steps: (1) compaction resulting from the rearrangement of the powder particles, increase in the contact surface of the particles, formation of more sparks, and increase in the thermal efficiency due to an increase in both pressure and temperature [17,19,20]; (2) First a decrease and then an increase in the displacement at 1100 °C: the initial decrease was indicative of the expansion caused by the gases produced by the evaporation of impurities and surface oxide contaminants in the presence of graphite additive. The second increase was caused by an increase in the pressure on the powder particles up to a final pressure of 40 MPa. Bulk deformation is caused by high temperature, neck growth among the particles, complete contact of particles, and noticeable compaction in this area; (3) A very slow increase in the slope of the curve and smooth displacement-time curves which are indicative of the complete compaction of this composite [21,22].

Apparently, the contact surface of the HfB_2 particles increased during the reaction of oxygen impurities (HfO_2 and B_2O_3) with SiC and graphite. As a result of this chemical reaction, gaseous products such as SiO, CO, and B_xO_y were produced which, prior to the production of gaseous products, caused the formation of the liquid phase and increased the sinterability of the HfB_2 powder [23].

Table 2 lists the physical and mechanical characteristics of the composite produce through SPS method. According to the results, the density of the obtained composite in this study was higher than the values reported by [24-27]. Since graphite can remove surface impurities on the SiC and HfB_2 particles and promote the densification of the composite, its addition to the composite would increase density and decrease the porosity percentage.

TABLE 2. Physical and mechanical properties of the HfB_2-30SiC-graphite composite

Material composition	HfB_2 average grain size (μm)	Relative density (%)	Apparent porosity (%)	Hardness (GPa)	K_{IC} (MPa m$^{1/2}$)	Strength (MPa)	Ref
HfB_2-20 vol. % SiC-10 vol. % $TaSi_2$	-	98.9	-	-	3.6	-	[24]
HfB_2-10 vol.% SiC	-	-	-	20.4	4.7		[25]
HfB_2-20 vol. % SiC-10 wt. % WC	6.9	99.1	-	10.6	3.36	563	[26]
HfB_2-20 vol. % SiC-20 vol. % HfC	2.57	98.8	-	21.07	3.72	585	[27]
HfB_2-15 vol. % SiC-15 vol. % $MoSi_2$	3.25	98.6	-	18	3	-	[28]
HfB_2-20 vol. % SiC-8 vol. % HfC	2.07	99.2	-	19	3.59	545	[29]
HfB_2-30 vol. % SiC-6 vol. % Graphite	HfB_2: 3.268 SiC: 2.155 Graphite: 0.125	99.39	0.61	10.16	4.73	464.12	Peresent work

The hardness of HfB_2-30 SiC-graphite composite was lower than that of HfB_2-SiC composite (18-20.4 GPa) in other researches [25,27-29]. Although this composite is characterized by a high density due to the inherent softness of graphite, its hardness is reduced.

The toughness and bending strength of HfB_2-20 SiC-graphite composite was higher and similar to those values reported in the literature, i.e., 4.65 MPa.m$^{1/2}$ and 465 MPa, respectively [24], mainly due to the laminar structure of the graphite and its role in siterability improvement of the composite. The effect of carbon fibers on the toughness of HfB_2 composites was also reported in [17].

Figure 2 shows the XRD pattern of the composite after the SPS process according to which, both HfB_2 and SiC phases can be observed in the samples, and there are no unwanted phases in the composites.
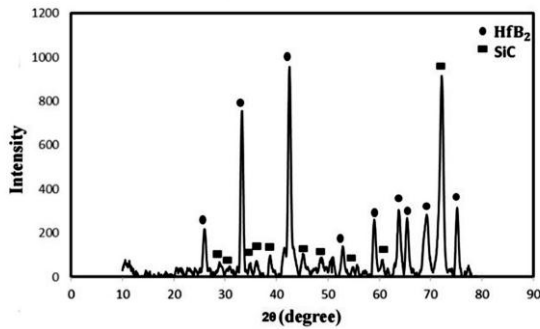
Figure 2. XRD pattern of the HfB$_2$-30 SiC-graphite composite sintered at 1950 °C for 10 min

Figure 3 shows the SEM images with elemental analysis (EDS) of the composite surface after the SPS process. According to EDS analysis, the dark and light areas represent the SiC and HfB$_2$ phases, respectively.
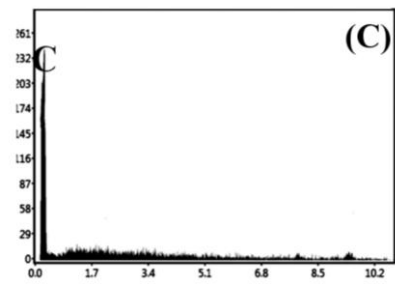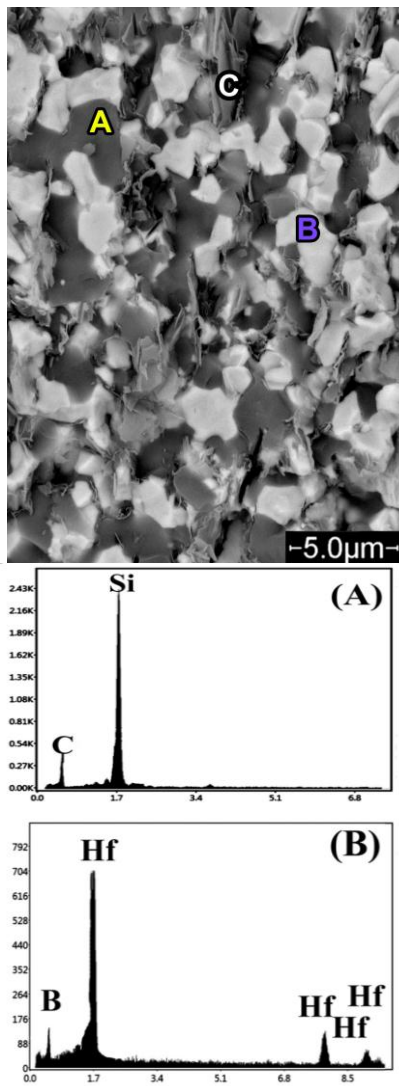

Figure 3. SEM images analysis (EDS) of the composite surface after the SPS process at 1950 °C for 10 min

Figure 4 depicts the SEM images of the fracture cross-section of the composite after the SPS process. The fracture surface of the sintered composite was a combination of the intergranular fractures. Particles pull-out and sharp edges observed in the images are possibly related to the intergranular fracture that occurred in grain boundaries (thin arrows). Certain areas, particularly in the compared surfaces with a typical grain growth compared to others, represent wide and smooth surfaces, indicating the intragranular fracture (thick arrows). An oxide layer on the surface of non-oxide particles (such as HfO$_2$, SiO$_2$, and B$_2$O$_3$) causes the generation of borosilicate glass phases. In their research work on the HfB$_2$-SiC composite sintered through hot pressing technique, Monteverde et al. stated that the glass phase in the SEM images was visible in the forms of coating, uniform and brittle fracture surface or a low thickness layer [30]. Such a glass phase was clearly visible in the SEM images of the cross-section of the composite prepared in the present research work (dashed flash).

In the cross-section images of HfB$_2$-SiC composites, graphite layers in different amounts can be observed in the cross-section, indicating that the graphite was not converted into new phases. Therefore, it can be concluded that the sintering and compressibility in the HfB$_2$-30 SiC-graphite systems was non-reactive.
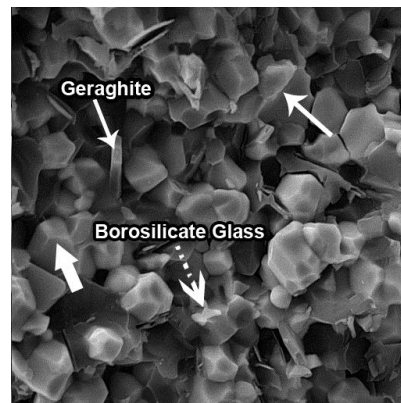

Figure 4. SEM of the fracture cross-section of the composite after the SPS process at 1950 °C for 10 min

Figure 5 presents the SEM image of the composite surface after oxidation at 1400 °C and different times according to which, the composite surface is coated with a glass layer. Oxidation of SiC particles according to reaction (2) at the temperatures above 1100 °C would form a glass layer of SiO_2 on the surface of the composite [31-35].

$$2\ SiC\ (s) +3\ O_2\ (g) = 2\ SiO_2\ (l) +2\ CO\ (g) \qquad (2)$$
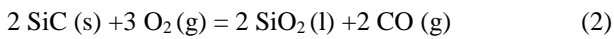
The glass layer is evenly distributed on the HfB_2-30 SiC-garaphite composite surface after oxidation for 12 and 16 h. As observed in the EDS analysis, the glass layer is evenly composed of Si and O. In addition, the white crystals of different sizes and shapes were found on the surface of composites after oxidation. According to the EDS analysis, the spherical crystals with high amounts of Hf and O and angular crystals with equal amounts of Hf and Si were HfO_2 and $HfSiO_4$ crystals, respectively.
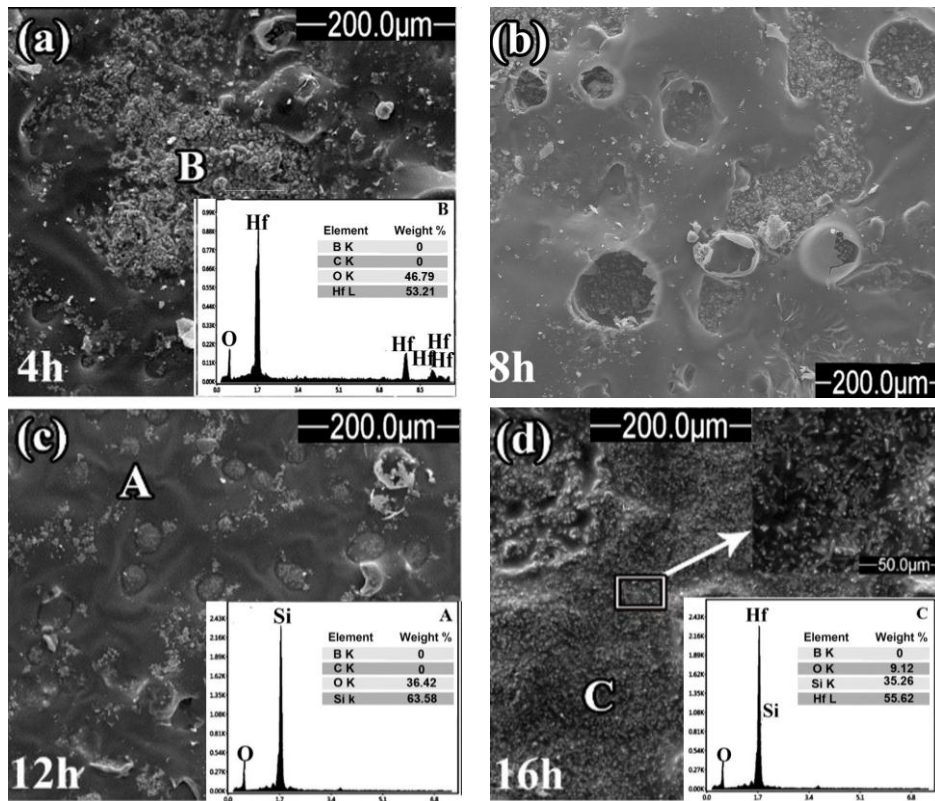

Figure 5. SEM image of the surface of the HfB_2-30 SiC-graphite composite after oxidation at 1400 °C for different Times, (a) 4 h, (b) 8 h, (c)12 h, and (d) 16 h

The formation of crystalline phases in the present study can be elaborated base on thermodynamic calculations (Figure 6) [31]. To be specific, followed by the formation of SiO_2 (reaction (2)) and HfO_2 (after oxidation at 800-1700 °C according to reaction (3)) [31], HfO_2 was first dissolved in the borosilicate melt, thus forming SiO_2-B_2O_3 (HSB) liquid in the glass layer.

As the oxidation process continued, the HSB liquid would flow from the top of the glass layer. In the case of B_2O_3 evaporation, HfO_2 particles were precipated from the HSB liquid. In addition, HfO_2 reacted with SiO_2 at temperatures above 1200 °C, according to reaction (4), thus forming $HfSiO_4$ particles [35].
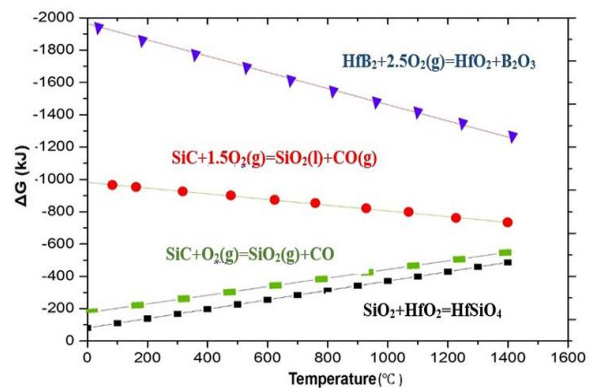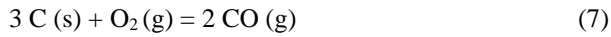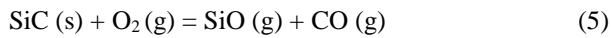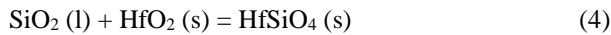

Figure 6. Gibbs free rnergy versus temperature for possible reactions in this study

$$2\ HfB_2\ (s) + 5\ O_2\ (g) = 2\ HfO_2\ (s) + 2\ B_2O_3\ (l) \qquad (3)$$

$$SiO_2\ (l) + HfO_2\ (s) = HfSiO_4\ (s) \qquad (4)$$

$$SiC\ (s) + O_2\ (g) = SiO\ (g) + CO\ (g) \qquad (5)$$

$$B_2O_3\ (l) = B_2O_3(g) \qquad (6)$$

$$3\ C\ (s) + O_2\ (g) = 2\ CO\ (g) \qquad (7)$$

Two types of bubbles were observed on the surface of this oxide layer some of which grew to the surface, yet the others could not find their way to the surface. Researchers believe that this layer cannot flow near these bubbles and cover the open bubbles owing to the high viscosity of the glass layer. These bubbles can be formed by the accumulation of gaseous products resulting from active oxidation of SiC at the high temperature of 1400 °C (reaction (5)) and B_2O_3 evaporation at the temprature of above 1100 °C (reaction (6)) and oxidation of graphite at 500 °C (reaction (6)) [2, 34].

Figure 7 illustrates the cross-section of the composite after the oxidation test at different times.

According to the EDS analysis (Figure 8), the first layer was rich in Si while the second one had moderate amount of Si and Hf.
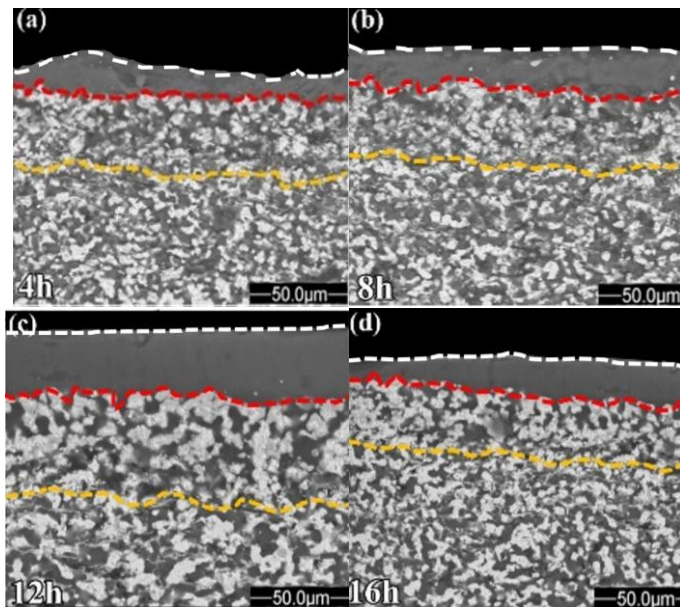

Figure 7. cross-section of the HfB$_2$-30 SiC-graphite composite sample after oxidation test for different times
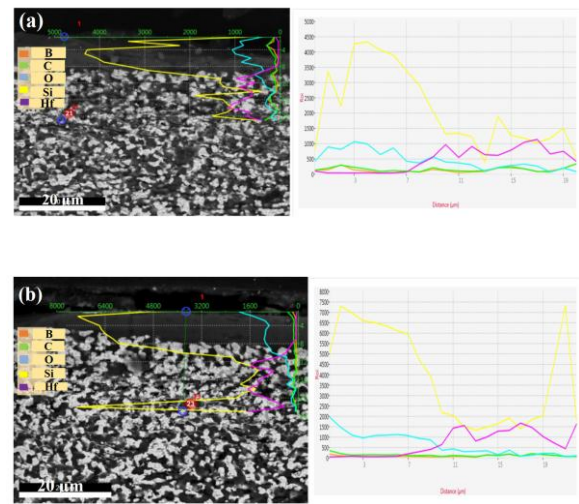

Figure 8. Line EDS analysis of the HfB$_2$-30 SiC-graphite composite sample after oxidation test for (a) 8 and (b) 16 h

Figure 9 shows the thickness of each layer formed on the surface of the HfB$_2$-30 SiC-graphite composite followed by conducting the oxidation test. The obtained results showed that followed by increasing the time of graphite oxidation during the oxidation process at 1400 °C and forming new channels for oxygen to better penetrate into the composite, the oxidation rate and thickness of SiO$_2$ rich layer would increase. Given that the formation of the thicker glass layer as a result of a decrease in the oxygen penetration into the composite after oxidation for 12 h, the thickness of SiO$_2$ rich layer would slowly increase. As observed in the EDS analysis (Figure 10), HfO$_2$, HfO$_x$C$_y$, and SiO$_x$C$_y$ phases were formed followed by oxidation for 12 h. Zapata et al. reported the formation of MeO$_x$C$_y$ (Si, Zr,Hf) after oxidation of MeB$_2$-SiC (Zr,Hf) composites at 1500 °C for 3 h [36,37].
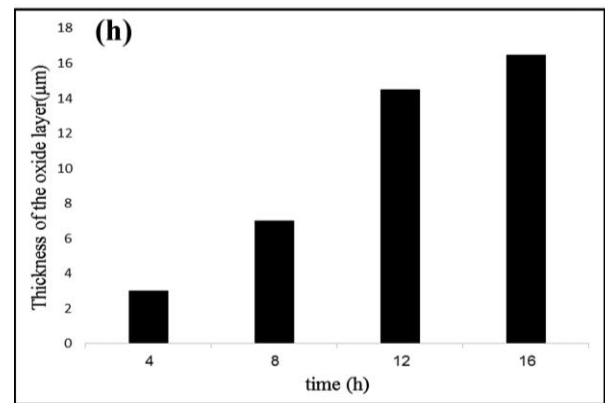

Figure 9. Thickness of the oxide layer formed on the surface after conducting the oxidation test at different times

MeO$_x$C$_y$ phases were proposed as the novel protective coatings for UHTCs in cases where the oxygen diffusion

coefficients were reduced, and oxidation resistance of composites was improved for a long exposure time. In this study, followed by the formation of the HfO_xC_y and SiO_xC_y phases and their oxidation, oxygen diffusion into the composite would decrease after 12 h. As a result, the thickness of the SiO_2 layer slowly increased. Therefore, it can be expected that the composite will follow a stabilized trend at long exposure times.
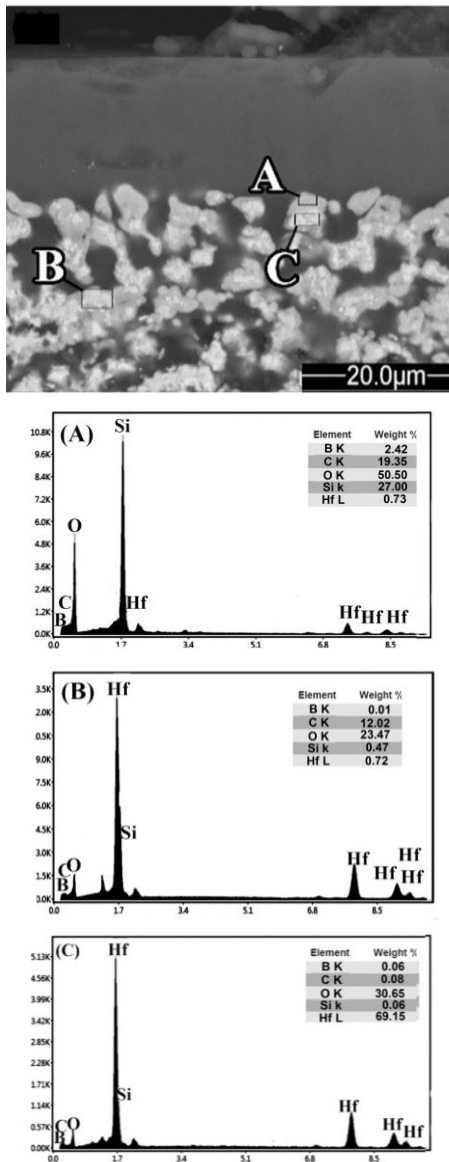

Figure 10. cross-section of the HfB_2-30 SiC-graphite composite sample after the oxidation test for 16 h

Figure 11 illustrates the oxidation kinetics of HfB_2–30 SiC–graphite composites oxidized at 1400 °C.

The oxidation mechanism is determined by the changes in the weight gain per unit surface area ($\Delta W/S$) as an oxidation time function.
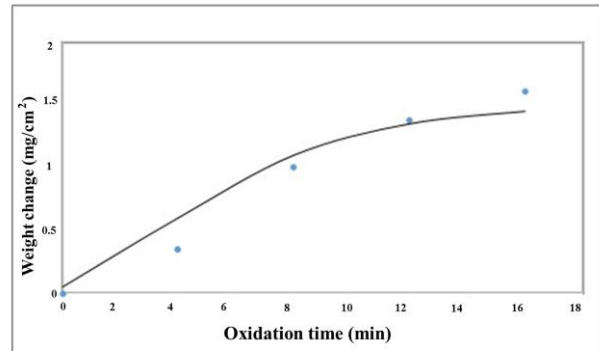

Figure 11. Oxidation kinetics of HfB_2-30 SiC-graphite composites oxidized at 1400 °C

The oxidation kinetic variables, x and k, are calculated using Equation (8):

$$(\Delta W/S)^x = kt \qquad (8)$$

where x is the oxidation exponent, and k the constant of the oxidation rate.

According to the literature, while the linear trend (x=1) is indicative of the reaction rate-controlled kinetics, the parabolic one (x=2) is indicative of the diffusion rate-controlled kinetics. The value of x in the current study was calculated as 1.563 which was indicative of a linear-parabolic behavior. While the linear oxidation kinetics were observed for 8 h, the parabolic oxidation kinetics were observed for up to 16 h. The thickness of the oxide scale rapidly increased 8 h past the oxidation, thus making the trend linear.

According to Figure 5, HfO_2 and $HfSiO_4$ were the main phases on the top oxide layer at the oxidation time of less than 12 h, suggesting that under this condition, the oxidation was controlled by the reaction rate. After 12 h of oxidation, the thickness of the oxide scale gradually increased, following a parabolic trend mainly due to the impact of the produced HfO_xC_y and SiO_xC_y phases that reduced the oxygen transport. With the development of these phases, the rate of oxidation began to increase steadily. As a result, the diffusion rate determined the oxidation rate. There was a barrier for oxygen diffusion in this stage. The oxidation rate was liner at first; however, after the formation of HfO_xC_y and SiO_xC_y phases, oxygen was used for oxidation of these phases. Consequently, the oxygen diffiusion rate in the bulk decreased, hence improvement in the oxidation resistance of the composite and gradual increase in the oxidation rate.

4. CONCLUSION

In the current research, HfB_2-30 vol. % SiC-6 vol. %

graphite composite was fabricated through SPS method. The obtained composite was charaterized by high relative density (99.39 %) and good mechanical properties (the toughness and strength values were obtained as 4.73 $MPa.m^{1/2}$ and 464.12 MPa, respectively). The oxidation behavior of the composite was studied at 1400 °C and different times. The thickness of the oxide layer formed on the surface of the HfB_2-30 SiC-graphite composite increased from 3.2 µm to 16.1 µm upon increasing the oxidation time. The composite exhibited a linear-parabolic behavior during the the oxidation test, and the oxidation exponent was obtained as 1.563. The results from the elemental analysis revealed that HfO_2 and $HfSiO_4$ were the main oxide specieses on the top oxide layer at the oxidation time below 12 h, suggesting that under this condition, the oxidation was controlled by the reaction rate. After oxidation for more 12 h, the thickness of the oxide scale slowly increased, thus making the trend parabolic mainly due to the impact of the decreasing oxygen diffusion on the formed HfO_xC_y and SiO_xC_y solid solutions. Of note, the oxidation was controlled by the diffusion rate. For this reason, it expected that the composite would follow a stabilized trend at long exposure times.

ACKNOWLEDGEMENTS

REFERENCES

1. Shojaie-Bahaabad, M., Hasani-Arefi, A., "Ablation properties of ZrC-SiC-HfB_2 ceramic with different amount of carbon fiber under an oxyacetylene flame", *Materials Research Express*, Vol. 7, No. 2, (2020), 025604. https://doi.org/10.1088/2053-1591/ab70db

2. Hassan, R., Kundu, R., Balani, K., "Oxidation behaviour of coarse and fine SiC reinforced ZrB_2 at re-entry and atmospheric oxygen pressures", *Ceramics International*, Vol. 46, No. 8, (2020), 11056-11065. https://doi.org/10.1016/j.ceramint.2020.01.125

3. Binner, J., Porter, M., Baker, B., Zou, J., Venkatachalam, V., Diaz, V. R., D'Angio, A., Ramanujam, P., Zhang, T., Murthy, T. S. R. C., "Selection, processing, properties and applications of ultra-high temperature ceramic matrix composites, UHTCMCs – a review", *International Materials Reviews*, Vol. 65, No. 7, (2019), 389-444. https://doi.org/10.1080/09506608.2019.1652006

4. Ghelich, R., Jahannama, M. R., Abdizadeh, H., Torknik, F. S., Vaezi, M. R., "Hafnium diboride nonwoven mats with porosity/morphology tuned via different heat treatments", *Materials Chemistry and Physics*, Vol. 248, (2020), 122876. https://doi.org/10.1016/j.matchemphys.2020.122876

5. Ni, D. W., Zhang, G. J., Kan, Y. M.,Wang, P. L., "Synthesis of monodispersed fine hafnium diboride powders using carbo/borothermal reduction of hafnium dioxide", *Journal of the American Ceramic Society*, Vol. 91, No. 8, (2008), 2709-2712. https://doi.org/10.1111/j.1551-2916.2008.02466.x

6. Wang, H., Lee, S. H., Kim, H. D., Oh, H. C., "Synthesis of ultrafine hafnium diboride powders using solution-based processing and spark plasma sintering", *International Journal of Applied Ceramic Technology*, Vol. 11, No. 2, (2014), 359-363. https://doi.org/10.1111/ijac.12016

7. Zou, J., Zhang, G. J., Kan, Y. M., Ohji, T., "Pressureless sintering mechanisms and mechanical properties of hafnium diboride ceramics with pre-sintering heat treatment", *Scripta Materialia*, Vol. 62, No. 3, (2010), 159-162. https://doi.org/10.1016/j.scriptamat.2009.10.014

8. Monteverde, F., Bellosi, A., "Efficacy of HfN as sintering aid in the manufacture of ultrahigh-temperature metal diborides-matrix ceramics", *Journal of Materials Research*, Vol. 19, No. 12, (2004), 3576-3585. https://doi.org/10.1557/JMR.2004.0460

9. Hu, D. L., Zheng, Q., Gu, H., Ni, D. W., Zhang, G. J., "Role of WC additive on reaction, solid-solution and densification in HfB_2-SiC ceramics", *Journal of the European Ceamic Society*, Vol. 34, No. 3, (2014), 611-619. https://doi.org/10.1016/j.jeurceramsoc.2013.10.007

10. Monteverde, F., "Hot pressing of hafnium diboride aided by different sinter additives", *Journal of Materials Science*, Vol. 43, No. 3, (2008), 1002–1007. https://doi.org/10.1007/s10853-007-2247-9

11. Mashayekh, S., Baharvandi, H. R., "Effects of SiC or $MoSi_2$ second phase on the oxide layers structureof HfB_2-based composites", *Ceramics International*, Vol. 43, No. 17, (2017), 15053-15059. https://doi.org/10.1016/j.ceramint.2017.08.031

12. Ren, X., Shang, T., Wang, W., Feng, P., Guo, L., Zhang, P., Li, Z., "Dynamic oxidation protective behaviors and mechanisms of HfB_2-20wt%SiC composite coating for carbon materials", *Journal of the European Ceramic Society*, Vol. 39, No. 6, (2019), 1955-1964. https://doi.org/10.1016/j.jeurceramsoc.2019.01.033

13. Guérineau, V., Vilmart, G., Dorval, N., Julian-Jankowiak, A., "Comparison of ZrB_2-SiC, HfB_2-SiC and HfB_2-SiC-Y_2O_3 oxidation mechanisms in air using LIF of BO_2 (g)", *Corrosion Science*, Vol. 163, (2019), 108278. https://doi.org/10.1016/j.corsci.2019.108278

14. Ghadami, S., Taheri-Nassaj, E., Baharvandi, H. R., Ghadami, F., "Effect of in situ VSi_2 and SiC phases on the sintering behavior and the mechanical properties of HfB_2-based composites", *Scientific Reports*, Vol. 10, No. 1, (2020), 1-13. https://doi.org/10.1038/s41598-020-73295-7

15. Simonenko, E. P., Simonenko, N. P., Lysenkov, A. S., Sevast'yanov, V. G., Kuznetsov, N. T., "Reactive Hot Pressing of HfB_2–SiC–Ta_4HfC_5 Ultra-High Temperature Ceramics", *Journal of Inorganic Chemistry*, Vol. 65, No. 3, (2020), 446-457. https://doi.org/10.1134/S0036023620030146

16. Simonenko, E. P., Simonenko, N. P., Nagornov, I. A., Sevastyanov, V. G., Kuznetsov, N.T., "Production and oxidation resistance of HfB_2–30 vol % SiC composite powders modified with $Y_3Al_5O_{12}$", *Russian Journal of Inorganic Chemistry*, Vol. 65, No. 9, (2020), 1416–1423. https://doi.org/10.1134/S003602362009020X

17. Guo, S., Naito, K., Kagawa, Y., "Mechanical and physical behaviors of short pitch-based carbon fiber-reinforced HfB_2–SiC matrix composites", *Ceramics International*, Vol. 39, No. 2, (2013), 1567–1574. https://doi.org/10.1016/j.ceramint.2012.07.108

18. Simonenko, E. P., Simonenko, N. P., Kolesnikov, A. F., Chaplygin, A. V., Lysenkov, A. S., Nagornov, I. A., Simonenko, T. L., Gubin, S. P., Sevastyanov, V. G., Kuznetsov, N. T., "Oxidation of graphene-modified HfB_2-SiC ceramics by supersonic dissociated air flow", *Journal of the European Ceramic Society*, Vol. 42, No. 1, (2022), 30-42. https://doi.org/10.1016/j.jeurceramsoc.2021.09.020

19. Shahriari, M., Zakeri, M., Razavi, M., Rahimipour, M. R., "Investigation on microstructure and mechanical properties of HfB_2-SiC-HfC ternary system with different HfC content prepared by spark plasma sintering", *International Journal of Refractory Metals and Hard Materials*, Vol. 93, (2020), 105350. https://doi.org/10.1016/j.ijrmhm.2020.105350

20. Emami, S. M., Salahi, E., Zakeri, M., Tayebifard, S. A., "Effect of composition on spark plasma sintering of ZrB_2–SiC–ZrC nanocomposite synthesized by SPS", *Ceramics International*, Vol. 43, No. 1, (2017), 111-115. https://doi.org/10.1016/j.ceramint.2016.09.118

21. Ghadami, S., Taheri-Nassaj, E., Baharvandi, H. R., Ghadami, F., "Improvement of mechanical properties of HfB_2^- based composites by incorporating in situ SiC reinforcement", *Scientific Reports*, Vol. 11, No. 1, (2021), 1-11. https://doi.org/10.1038/s41598-021-88566-0

22. Ghasali, E., Pakseresht, A., Safari-kooshali, F., Agheli, M., Ebadzadeh, T., "Investigation on microstructure and mechanical behavior of Al-ZrB_2 composite prepared by microwave and spark plasma sintering", *Materials Science and Engineering: A*, Vol. 627, (2015), 27-30. https://doi.org/10.1016/j.msea.2014.12.096

23. Grigoriev, S. N., Pristinskiy, Y., Soe, T. N., Malakhinsky, A., Mosyanov, M., Podrabinnik, P., Smirnov, A., Solís Pinargote, N. W., "Processing and characterization of spark plasma sintered SiC-TiB_2-TiC powders", *Materials*, Vol. 15, No. 5, (2022), 1946. https://doi.org/10.3390/ma15051946

24. Monteverde, F., "Ultra-high temperature HfB_2–SiC ceramics consolidated by hot-pressing and spark plasma sintering", *Journal of Alloys and Compounds*, Vol. 428, No. 1-2, (2007), 197-205. https://doi.org/10.1016/j.jallcom.2006.01.107

25. Wang, H., Lee, S. H., Feng, L., "HfB_2-SiC composite prepared by reactive spark plasma sintering", *Ceramics International*, Vol. 40, No. 7, (2014), 11009–11013. https://doi.org/10.1016/j.ceramint.2014.03.107

26. Yuan, Y., Liu, J. X., Zhang, G. J., "Effect of HfC and SiC on microstructure and mechanical properties of HfB_2-based ceramics", *Ceramics International*, Vol. 42, No. 6, (2016), 7861-7867. https://doi.org/10.1016/j.ceramint.2016.01.067

27. Ghadami, S., Taheri-Nassaj, E., Baharvandi, H. R., "Novel HfB_2-SiC-$MoSi_2$ composites by reactive spark plasma sintering", *Journal of Alloys and Compounds*, Vol. 809, (2019), 151705. https://doi.org/10.1016/j.jallcom.2019.151705

28. Sakkaki, M., Moghanlou, F. S., Vajdi, M., Shahedi Asl, M., "Numerical simulation of heat transfer during spark plasma sintering of zirconium diboride", *Ceramics International*, Vol. 46, No. 4, (2020), 4998-5007. https://doi.org/10.1016/j.ceramint.2019.10.240

29. Shahedi Asl, M., "Microstructure, hardness and fracture toughness of spark plasma sintered ZrB_2–SiC–C_f composites", *Ceramics International*, Vol. 43, No. 17, (2017), 15047-15052. https://doi.org/10.1016/j.ceramint.2017.08.030

30. Monteverde, F., "Progress in the fabrication of ultra-high-temperature ceramics: "In situ" synthesis, microstructure and properties of a reactive hot-pressed HfB_2-SiC composite", *Composites Science and Technology*, Vol. 65, No. 11-12, (2005), 1869-1879. https://doi.org/10.1016/j.compscitech.2005.04.003

31. Ghadami, S., Taheri-Nassaj, E., Baharvandi, H. R., Ghadami, F., "Effect of in situ SiC and $MoSi_2$ phases on the oxidation behavior of HfB_2- based composites", *Ceramics International*, Vol. 46, No. 12, (2020), 20299-20305. https://doi.org/10.1016/j.ceramint.2020.05.116

32. Wang, P., Li, H., Sun, J.,Yuan, R., Zhang, L., Zhang, Y., Li, T., "The effect of HfB_2 content on the oxidation and thermal shock resistance of SiC coating", *Surface and Coatings Technology*, Vol. 339, (2018), 124-131. https://doi.org/10.1016/j.surfcoat.2018.02.029

33. Simonenko, E. P., Simonenko, N. P., Gordeev, A. N., Kolesnikov, A. F., Chaplygin, A. V., Lysenkov, A. S., Nagornov, I. A., Sevastyanov, V. G., Kuznetsov, N. T., "Oxidation of HfB_2-SiC-Ta_4HfC_5 ceramic material by a supersonic flow of dissociated air", *Journal of the European Ceramic Society*, Vol. 41, No. 2, (2021), 1088-1098. https://doi.org/10.1016/j.jeurceramsoc.2020.10.001

34. Gürcan, K., Derin, B., Ayas, E., "Effect of SiC particle size on the microstructural, mechanical and oxidation properties of In-situ synthesized HfB_2-SiC composites", *Politeknik Dergisi*, Vol. 24, No. 2, (2021), 503-510. https://doi.org/10.2339/politeknik.682256

35. Ren, X., Mo, H., Wang, W., Feng, P., Guo, L., Li, Z., "Ultrahigh temperature ceramic HfB_2-SiC coating by liquid phase sintering method to protect carbon materials from oxidation", *Materials Chemistry and Physics*, Vol. 217, (2018), 504–512. https://doi.org/10.1016/j.matchemphys.2018.07.018

36. Zapata-solvas, E., Jayaseelan, D. D., Brown, P. M., Lee, W. E., "Effect of La_2O_3 addition on long-term oxidation kinetics of ZrB_2–SiC and HfB_2–SiC ultra-high temperature ceramics", Journal of the European Ceramic Society, Vol. 34, (2014), 3535–3548. https://doi.org/10.1016/j.jeurceramsoc.2014.06.004

37. Guo, S., "Oxidation and strength retention of HfB_2–SiC composite with La_2O_3 additives", *Advances in Applied Ceramics*, Vol. 119, No. 4, (2020), 218-223. https://doi.org/10.1080/17436753.2020.1755510